Available online at www.sciencedirect.com

ScienceDirect

journal homepage: www.elsevier.com/locate/he

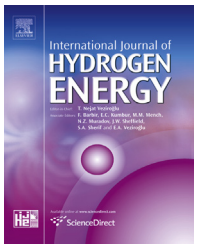

Durable ethanol steam reforming in a catalytic membrane reactor at moderate temperature over cobalt hydrotalcite

R. Espinal [a], A. Anzola [b], E. Adrover [b], M. Roig [a], R. Chimentao [c], F. Medina [c], E. López [b], D. Borio [b], J. Llorca [a,*]

[a] Institut de Tècniques Energètiques and Centre for Research in NanoEngineering, Universitat Politècnica de Catalunya, Diagonal 647, Ed. ETSEIB, 08028 Barcelona, Spain

[b] Planta Piloto de Ingeniería Química (UNS-CONICET), Camino la Carrindanga Km 7, Bahía Blanca 8000, Argentina

[c] Escola Tècnica Superior d'Enginyeria Química, Universitat Rovira i Virgili, Av. Països Catalans 26, 43007 Tarragona, Spain

ARTICLE INFO

Article history:
Received 24 March 2014
Received in revised form
10 May 2014
Accepted 19 May 2014
Available online 14 June 2014

Keywords:
Ethanol steam reforming
Cobalt
Hydrotalcite
Pd dense membrane
Catalytic membrane reactor

ABSTRACT

Ethanol steam reforming has been carried out in a catalytic membrane reactor consisting of cobalt hydrotalcite $[Co_2Mg_4Al_2(OH)_{16}]CO_3 \cdot 4H_2O$-derived catalyst doped with potassium supported over cordierite and a composite Pd–Ag selective membrane. No sweep gas has been used, therefore, pure hydrogen has been obtained in the permeate stream, which has been maintained at atmospheric pressure. The configuration with the catalyst bed packed around the membrane has shown values of STP $L_{H_2,\ permeate}\ mL_{ETOH,\ liquid}^{-1}\ g_{cat}^{-1}$ up to 3 times higher than the observed for the staged membrane reactor, where the catalyst has been placed in-series with the membrane. The influence of the temperature (673–873 K), the water-ethanol ratio (S/C = 1.8–3) and the retentate pressure (1–18 bar) on different performance parameters such as the hydrogen production and the pure hydrogen recovery has been evaluated. No carbon accumulation has been observed by SEM and XPS after 650 h operation.

Introduction

On-site hydrogen generation from various liquid fuels as an alternative to direct hydrogen storage is envisioned as one of the key points for the use of proton exchange membrane fuel cells (PEMFC) for the market of power sources for portable and mobile applications [1,2]. Among liquid fuels that are currently considered, ethanol is advantageous over other conventional substrates because it is readily available, easy to obtain from biomass and to transport, CO_2-neutral and safe to handle [3,4]. In recent years, numerous catalyst formulations have been studied intensively for ethanol steam reforming (ESR) aiming at the generation of hydrogen [5–8]:

$$C_2H_5OH + 3H_2O \leftrightarrows 6H_2 + 2CO_2 \quad (1)$$

An efficient catalyst for hydrogen production from ethanol has to dissociate the C–C bond, maintain a low CO concentration and be stable under catalytic operation. A survey of the

* *Corresponding author*. Institut de Tècniques Energètiques, Universitat Politècnica de Catalunya, Av. Diagonal 647, Ed. ETSEIB, 08028 Barcelona, Spain. Tel.: +34 93 401 17 08; fax: +34 93 401 71 49.
E-mail address: jordi.llorca@upc.edu (J. Llorca).
http://dx.doi.org/10.1016/j.ijhydene.2014.05.127

literature reveals that noble metal-based catalysts perform well for ESR [9–11]. They are stable and exhibit high activity. However, they are expensive and need high temperatures to be active. The main reaction mechanism involves the decomposition of ethanol into a mixture of hydrogen, carbon monoxide and methane, followed by the steam reforming of the produced methane. Additionally, the water gas shift reaction balances CO and CO_2 rendering extra hydrogen amounts. A similar reaction network is found over nickel catalysts, which are inexpensive but usually suffer from sintering and deactivation by carbon deposition.

Cobalt-based catalysts can operate at lower temperature levels when compared with noble metal-based catalysts since they do not yield methane as an intermediate species in the reaction mechanism, which can only be reformed at high temperature [12–38]. Over cobalt-based catalysts, ethanol is first dehydrogenated into a mixture of hydrogen and acetaldehyde (Eq. (2)), and then acetaldehyde reacts with steam to yield mainly hydrogen and carbon oxides (Eq. (3)), which participate in the WGS (Eq. (4)), or decompose into carbon monoxide and methane (Eq. (5)), which in turn undergo steam reforming (Eq. (6)):

$$C_2H_5OH \leftrightarrows H_2 + CH_3CHO \quad (2)$$

$$CH_3CHO + H_2O \leftrightarrows 3H_2 + 2\,CO \quad (3)$$

$$CO + H_2O \leftrightarrows H_2 + CO_2 \quad (4)$$

$$CH_3CHO \leftrightarrows CH_4 + CO \quad (5)$$

$$CH_4 + H_2O \leftrightarrows 3H_2 + CO \quad (6)$$

An important advantage of conducting the ESR at lower temperature is that the WGS equilibrium favors the formation of hydrogen and CO_2 at the expense of CO and water (Eq. (4)), thus maximizing the production of H_2 and reducing the volume of the WGS units normally implemented downstream the reformer (or even using a single WGS reactor). The heat transfer management of the fuel processor design is simplified as well. However, in contrast to noble metal-based systems, most cobalt catalysts suffer from severe deactivation during ESR due to extensive carbon deposition, particularly under realistic loads of ethanol. Essential for this matter is the understanding of the role of cobalt oxidation state. Accurate in situ studies have revealed that Co metal particles are formed easily under reaction conditions, which rapidly detach from the catalyst support and originate carbon nanotubes, nanofibers and platelets. At the same time, selectivity to methane and higher hydrocarbons increases at the expense of the reforming products (H_2 and CO_x). Recently, we have reported that catalysts derived from Co/Mg/Al hydrotalcites are active for ESR at 823 K and do not accumulate carbon because no metallic cobalt is formed under reaction conditions [39]. This interesting result allows designing catalysts containing cobalt for ESR without coke deposition (no metallic cobalt) by placing in appropriate environments Co^{2+} active species. Over K^+-doped hydrotalcite-derived cobalt catalysts we have reported stable operation under high loads of ethanol and commercial bioethanol [40].

The use of catalytic membrane reactors (CMR), where the generation and separation of hydrogen take place simultaneously, appears as an attractive approach to further simplify on-site/on-demand reformers. In addition, the extraction of hydrogen from the reaction medium that occurs in CMR equipped with H_2-selective membranes leads to an equilibrium shift in the reforming reactions and enables attaining enhanced hydrogen yields when compared with conventional reactors operating under the same conditions [41]. With respect to a classical configuration consisting of a reactor unit in series with a separation unit, CMR represent a modern configuration in which an integrated reaction/separation unit has many potential advantages: reduced capital costs, improved yields and selectivities and drastically reduced downstream separation costs [42,43].

Among CMRs, palladium-based membrane reactors fulfill the requirements to obtain an ultra-pure hydrogen stream suitable for PEMFC feeding. Via innovative techniques, such as cold-rolling and diffusion welding developed at several laboratories and companies, robust Pd-based thin wall tubes less than 0.05 mm in wall thickness have been produced [44] and their complete hydrogen selectivity and durability have been demonstrated in long-term tests [45]. Today, numerous catalytic membrane reactors designs are available for producing high hydrogen throughputs in compact reforming systems [46,47]. In addition, the retentate gas outcoming the membrane reactor can be used as a fuel source for a catalytic combustor to provide a thermally self-sustainable operation [48].

Pd alloy membranes have been used in CMR mainly for WGS and steam reforming reactions of methane and methanol, but their use in the steam reforming of ethanol is relatively new [49–55]. The ethanol steam reforming catalysts used in these studies were noble metals-based (e.g., Ru, Rh, Pt and Pd). Concerning the use of cobalt-based catalysts for ESR in catalytic membrane reactors, Iulianelli et al. conducted ESR over commercial Co/Al_2O_3 [56,57] supplying a diluted reactant mixture of ethanol:water with N_2. Several operational parameters such as temperature, pressure, sweep-gas flow and load were evaluated and hydrogen yield and recovery values as high as 60% and 95%, respectively, were reached at 673 K, 3 bar, SF = 25.2 (countercurrent flow) and WHSV = 0.2 h^{-1}. Lim et al. [58,59] and Yun et al. [60] studied ESR over Na–Co/ZnO over different composite membranes, i.e., SiO_2–Al_2O_3, Pd–Cu/SiO_2–Al_2O_3 and ultrathin Pd-or Pd–Cu/α-alumina. In these works, the reactant mixture of ethanol:water was diluted with Ar. Moreover, a sweep gas (Ar) was employed in order to increase the permeation driving force. The commercial Co/Al_2O_3 catalyst was tested at 673 K in a porous stainless steel (PSS) supported Pd membrane reactor with the aim of investigating the influence of the membrane characteristics as well as of the reaction pressure from 3 to 8 bar by Basile et al. [61]. Hydrogen recovery of about 50% was reached under complete ethanol conversion. Recently, a Co/Al_2O_3 catalyst has been used in a PSS membrane reactor at 673 and 8–12 bar for simulating bio-ethanol steam reforming by using a mixture of water-ethanol-acetic acid and glycerol with 1:13:0.18:0.04 molar ratio [62]. About 94% of bio-ethanol conversion was obtained at 12 bar and GHSV = 800 h^{-1}, with 40% hydrogen yield and 40% hydrogen recovery. Finally, Domínguez et al. [63] studied the

ESR in a CMR over cobalt talc at 598–673 K and 5–15 bar. In addition to an improvement of the hydrogen yield, the CMR showed a rapid response to changes in the ethanol-water mixture load; a constant hydrogen flow was obtained after 2s following variations of ±10%. One of the main issues of conducting the ESR in a CMR, however, is deactivation of the catalyst by deposition of carbon residues. The continuous removal of hydrogen from the reactor promotes carbon deposition onto the surface of the catalyst [64]. On the other hand, carbon deposition affects negatively the hydrogen permeation by covering the membrane surface and lowering the hydrogen permeating flux. In addition, carbon atoms penetrate into the Pd lattice causing membrane failure owing to the concomitant expansion of the Pd lattice. The works reported in the literature concerning the use of cobalt-based catalysts for ESR in CMRs [56,57,59,63] do not give information about the stability of the catalyst except for Lim et al. [58], who achieved stable ethanol conversion and product selectivity for 30 h at 623 K employing a Na–Co/ZnO catalyst. The lack of information about catalyst stability is really a critical point that deserves attention for a practical use. No matter how active a catalyst, if stable operation is not reasonable achieved then its full potential will not be reached.

Here, we extend our work on hydrotalcite-derived cobalt catalysts by studying their performance in a catalytic membrane reactor equipped with a Pd–Ag membrane to obtain PEM fuel cell-grade hydrogen (1 atm, no sweep gas). Different reactor configurations, temperature (673–873 K), pressure (1–18 bar), ethanol load and steam-to-carbon (S/C = 1.8–3) ratios have been tested. It is important to highlight that under these reaction conditions, i.e., high pressures, low steam to carbon ratio, non-diluted reaction mixtures and hydrogen permeation, carbon formation is favored. For the first time, we report stable ESR operation (650 h) at moderate temperature in a catalytic membrane reactor over a cheap and affordable cobalt catalyst, which constitutes an important innovation in the development of fuel reformers for providing PEM fuel cell-grade hydrogen.

Materials and methods

Preparation of catalyst

The Co/Mg/Al hydrotalcite with formula $[Co_2Mg_4Al_2(OH)_{16}]CO_3\cdot 4H_2O$ was prepared as described elsewhere by co-precipitation from aqueous solutions of $Co(NO_3)_2\cdot 6H_2O$, $Mg(NO_3)_2\cdot 6H_2O$ and $Al(NO_3)_3\cdot 9H_2O$ and 2M NaOH alkaline solution at a constant pH of 10 ± 0.5. The resulting solid was thoroughly washed, dried at 373 K and calcined at 823 K for 12 h to obtain the hydrotalcite-derived mixed oxide. Potassium addition to the calcined hydrotalcite (1.0 wt.% referred to the nominal cobalt content) was accomplished by impregnation with KOH aqueous solution. The resulting catalyst was dried at 373 K and calcined at 823 K for 4 h.

The catalyst powder was deposited onto cordierite pieces ($Al_3Mg_2AlSi_5O_{18}$, 400 cells per square inch, Rauschert Company) by washcoating [39,40]. A 5:1 molar mixture of polyvinyl alcohol (PVA) and acetic acid was used as binding agent. The resulting catalytic cordierite pieces were dried at 373 K and calcined at 823 K for 4 h. The washcoating procedure was repeated until the catalyst loading was ca. 5% with respect to the cordierite support.

Characterization

X-ray diffraction (XRD) patterns were collected between 10 and 90° of 2θ with a step width of 0.02° and a step time of 1 s using a Bruker D8 instrument equipped with Cu Kα incident radiation ($\lambda = 1.5404$ Å) and a graphite monochromator.

The microstructure, morphology, and composition of the catalyst layer were studied with a Zeiss NEON40 crossbeam scanning electron microscope (SEM) operated at 5 kV and equipped with energy dispersive X-ray analysis (EDX).

Surface characterization was done with X-ray photoelectron spectroscopy (XPS) on an SPECS system equipped with an Al anode XR50 source operating at 150 mW and a Phoibos 150 MCD-9 detector. The pressure in the analysis chamber was below 10^{-7} Pa. The area analyzed was about 2 mm × 2 mm. The pass energy of the hemispherical analyzer was set at 25 eV and the energy step was set at 0.1 eV. Charge stabilization was achieved by using an SPECS Flood Gun FG 15/40. The following sequence of spectra was recorded: survey spectrum, C 1s, Co 2p, Al 2p, Mg 2p and C 1s again to check for charge stability as a function of time and the absence of degradation of the sample during the analyses. Data processing was performed with the CasaXPS program (Casa Software Ltd., UK). The binding energy (BE) values were referred to the C 1s peak at 284.8 eV.

Reaction tests

The functionalized cordierite pieces described above were implemented in a membrane reactor machined in stainless steel measuring 230 mm tall and 22 mm OD (Reb Research & Consulting). A feed evaporation conduit was welded around the reactor. The Pd–Ag membrane (30 μm active layer thickness over PSS) was a 76 mm tall, 1/8″ diameter, pine-hole free, dead-end tube with a total area of 7.1 cm^2. Two different design configurations were selected for the catalytic membrane reactor as shown in Fig. 1. First, the catalytic honeycombs (9 pieces, 1.32 g total catalyst load) were disposed in-series into the reactor followed by the membrane tube, resulting in a staged membrane reactor (SR) (Fig. 1A). In the second configuration (Fig. 1B), a fraction of the same catalytic honeycombs were crushed into small pieces (mean particle diameter 0.5 mm) and distributed around the membrane tube, resulting in a membrane reactor (MR) (0.46 g total catalyst load). Occasionally, the membrane outlet was blocked to represent the operation of a conventional fixed bed reactor (CR), i.e., without separation. The liquid feed mixture of ethanol and water was introduced with a Knauer Smartline HPLC pump. The retentate pressure was adjusted by a manually-operated back-pressure regulator. No pressure regulation was implemented on the permeate side (atmospheric pressure). No sweep gas was used, therefore, pure hydrogen was obtained in the permeate stream. The gaseous products of the retentate were analyzed by online gas chromatography (Agilent 3000A MicroGC) using MS 5Å, PlotU and Stabilwax columns and TCD detectors, as well as the

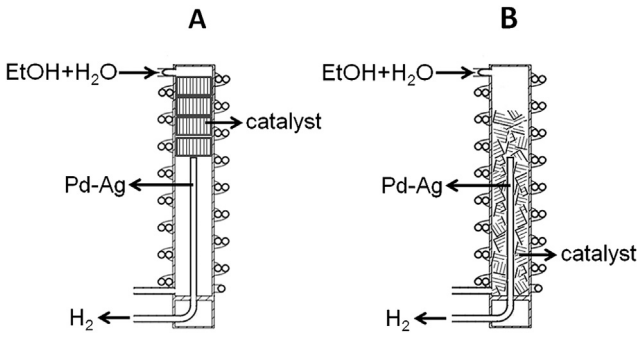

Fig. 1 – Scheme of the two membrane reactor configurations tested. (A) Staged membrane reactor (SR); (B) Catalytic membrane reactor (MR).

permeate to verify the selectivity of the membrane separation towards hydrogen. Calibration of gas concentrations was accomplished by using appropriate standards. Total volumetric flowrates of both permeate (Bronkhorst EL-FLOW) and dry retentate streams (bubble meter) were measured. By measuring under steady-state conditions and in a precise period of time both the composition and flowrate of the gaseous outlet streams as well as the volume of liquid condensed from the retentate flow we verified the correct closure of the mass balance and carbon balance. All the experiments were repeated at least twice and for each operational condition at least five different analyses were performed. Before the reaction, pure gas permeation tests were carried out on the reactor membrane, which showed that the selectivity towards hydrogen was infinite and that both Sieverts' and Arrhenius' laws were followed. The apparent activation energy for H_2 permeation was found to be 10.3 kJ mol^{-1} (±1.5 kJ mol^{-1} considering the 95% confidence limits), in agreement with values reported through the literature for membranes of similar characteristics [65–67].

Results and discussion

Catalyst characterization

The X-ray diffraction (XRD) profiles of the Co/Mg/Al hydrotalcite and the calcined catalyst doped with potassium (not shown) exhibited the characteristic peaks of the hydrotalcite structure (2θ at ca. 10.8, 22.5, 34.1, 38.4, 45.3, 60.2 and 61.8°) and cobalt or magnesium spinel (2θ at ca. 18.9, 31.5, 37.0, 44.4, 55.5, 59.2 and 65.0°), respectively, in accordance to previous studies [39,40].

Scanning electron microscopy (SEM) was carried out directly over the cordierite pieces loaded with catalyst as prepared as well as after the ethanol steam reforming tests performed in this study, which accounts for more than 650 h Fig. 2A shows a representative SEM image of the fresh catalyst. The sample is comprised mostly by rounded particles of about 20–40 nm in diameter, although several larger platelets are also visible. According to XRD and previous studies [39], the small, rounded particles are ascribed to cobalt spinel, whereas larger particles with platelet morphology correspond to mixed oxides coming from hydrotalcite calcination. Fig. 2B shows a SEM image of the catalyst after ESR for 650 h (at the end of the experiments). It is observed that the size of spinel particles decrease under ESR conditions, which now measure about 10–20 nm in diameter, and that the amount of hydrotalcite platelets increases after reaction. This is explained in terms of reconstruction of the catalyst due to rehydration under steam during ESR conditions, as observed previously [39]. What merits to be highlighted is the total absence of carbon deposition after 650 h of reaction. This is an outstanding result taking into account that low S/C ratios have been selected for approaching real operation (S/C = 1.8–3) and also that in a catalytic membrane reactor the partial pressure of hydrogen is lower than that in a conventional reactor due to hydrogen permeation through the membrane, which favors carbon deposition.

In order to definitely rule out the presence of carbon accumulation onto the catalyst after the ESR tests, we recorded the XP spectra of the surface of both the fresh catalyst and the used one (XPS is a surface sensitive technique and also very sensitive to carbon). The concentration of carbon on the catalysts was virtually identical in both cases (C/Co = 0.17 and 0.12, C/(Al + Mg) = 0.10 and 0.11 before and after reaction, respectively), thus confirming that no carbon accumulation occurred during ESR operation in the membrane reactor. We have reported previously by using in-situ spectroscopic techniques [44] that the presence of isolated Co centers in this catalyst during conventional ESR (packed bed reactor, atmospheric pressure, no separation membrane) is responsible for such extraordinary stability. Therefore, these catalytically active centers are likely preserved under ESR in the CMR as well.

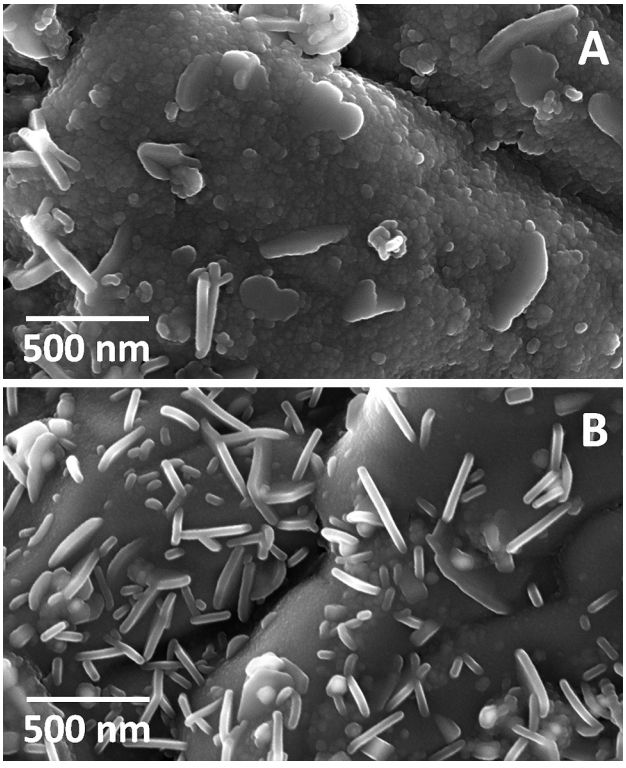

Fig. 2 – Scanning electron microscopy (SEM) images of the fresh catalyst (A) and the catalyst after ESR in the catalytic membrane reactor for 650 h (B).

Staged membrane reactor

As explained in the experimental section, two configurations for the catalyst and the Pd–Ag separation membrane were tested in the same reactor under similar reaction conditions (see Fig. 1). In all cases, ethanol conversion was complete and the only products detected by gas chromatography were H_2, CH_4, CO and CO_2. No acetaldehyde (the first step in ethanol reforming over Co-based catalysts, Eq. (2)), acetone (which is formed via condensation of acetaldehyde) or C_{2+} hydrocarbons were detected. The total amounts of H_2, CO_2, CO and CH_4 obtained in the staged configuration at atmospheric pressure and different reaction conditions were always fairly identical to those obtained previously for catalytic honeycombs loaded with the same catalyst in a fixed bed reactor [40], confirming reproducibility.

The effect of temperature on the selectivity values on a dry basis at 10 bar is shown in Fig. 3A. The amount of hydrogen increased with temperature at the expense of methane, which may be explained in terms of methane steam reforming (Eq. (6)). On the other hand, as temperature was increased, the reverse water gas shift reaction was favored and the amount of CO increased progressively at the expense of CO_2, according to the WGS equilibrium (Eq. (4)). Pressure had a stronger effect on the distribution of products of the reaction. Fig. 3B shows the selectivity values on a dry basis obtained at a fixed temperature of 833 K. The selectivity towards methane increased with pressure at the expense of hydrogen, which may be explained in terms of the Le Chatelier's principle, since the consumption of moles of H_2 and CO is favored with pressure to yield CH_4 (methanation reaction, see reverse of Eq. (6)).

Fig. 4 reports the amount of hydrogen permeated through the membrane as influenced by temperature and pressure in the SR design. As expected, pressure affected strongly the separation of hydrogen at each temperature. The increase of hydrogen flowrate through the membrane is explained in terms of the hydrogen permeation driving force due to the difference in hydrogen pressure at both sides of the membrane, as expected from Sieverts' equation. The larger the pressure difference of hydrogen in the retentate and permeate sides, the larger the permeated hydrogen amount per unit membrane area, this effect clearly dominating up to intermediate pressures (i.e., $P < 10$ bar). However, at higher pressures ($10 < P < 14$ bar), the curves of permeated hydrogen tend to attenuate. This is due to the fact that two conflicting effects occurred simultaneously. On one hand, pressure favored hydrogen permeation through the membrane and, therefore, a higher hydrogen permeating flux. On the other hand, high pressure values resulted in a decrease of the total production of hydrogen ($F^*_{H_2} = F_{H_2,\text{retentate}} + F_{H_2,\text{permeate}}$). This is a direct consequence of the thermodynamics of the reaction since the complete ethanol steam reforming reaction proceeds with a strong increase of the mole number (Eq. (1)). Thus, as pressure increases, the membrane located downstream the reactor is fed with gaseous mixtures containing lower molar fractions of H_2. The effect of temperature on the permeated hydrogen flowrate is also reported in Fig. 4. The increase of the operating temperature originates two effects, both resulting in an increase of the total amount of hydrogen permeated. Higher

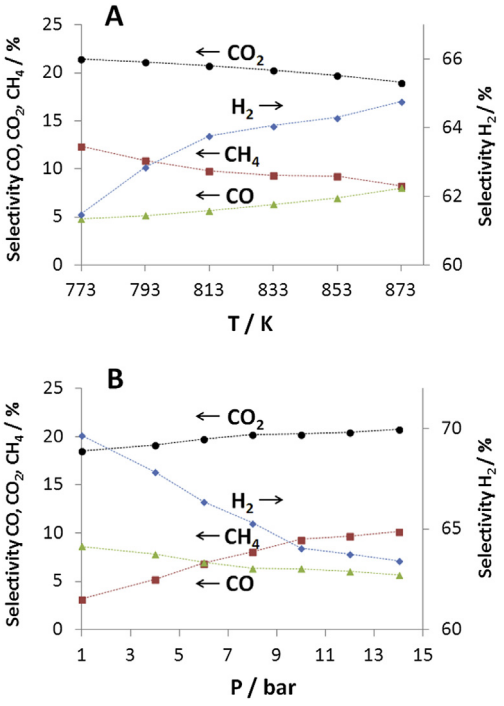

Fig. 3 – Staged membrane reactor configuration: (A) Effect of temperature on the selectivity values at 10 bar under steady state, $Q_{liq}/W = 13.6$ ml g_{cat}^{-1} h^{-1} and S/C = 2.4; (B) Effect of pressure on the selectivity values at 833 K under steady state, $Q_{liq}/W = 13.6$ ml g_{cat}^{-1} h^{-1} and S/C = 2.4.

temperatures favor both the total hydrogen production by the reforming reaction and also the permeation through the Pd–Ag membrane as this is a temperature-activated process.

Catalytic membrane reactor

Fig. 5 shows a comparison of the performance of the two different reactor configurations tested, i.e., SR and MR. Total

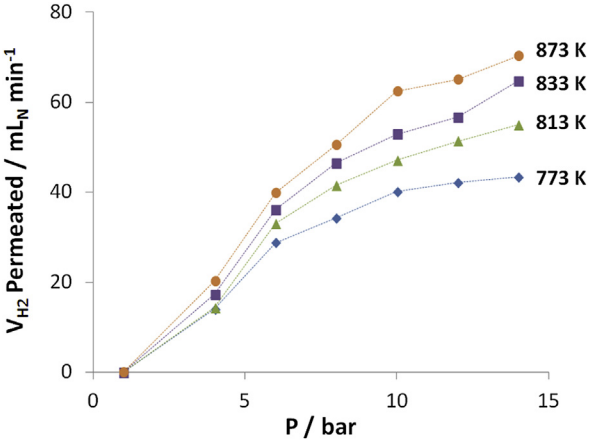

Fig. 4 – Staged membrane reactor configuration: Volumetric flowrate of hydrogen permeated at $Q_{liq}/W = 13.6$ ml g_{cat}^{-1} h^{-1} and S/C = 1.8 under different temperature and pressure values at steady state.

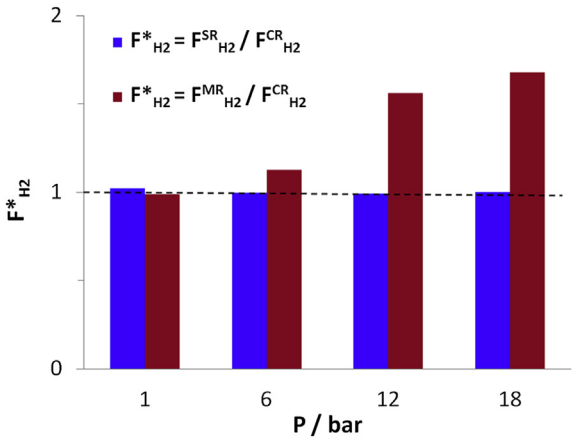

Fig. 5 – Influence of the reactor configuration on H_2 production under steady state at different pressures. T = 773 K, S/C = 3. SR = staged membrane reactor, MR = membrane reactor, CR = catalytic reactor without membrane separation.

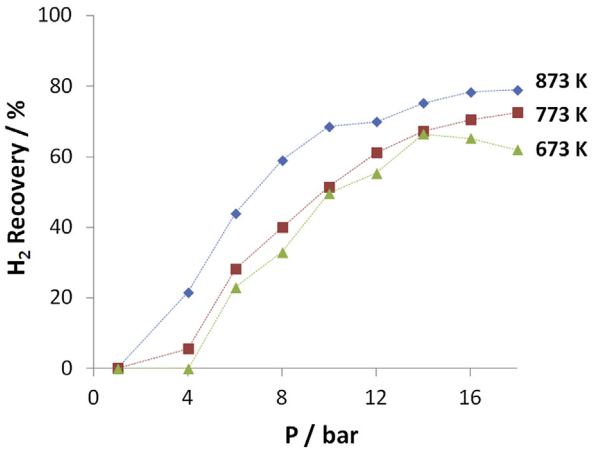

Fig. 6 – H_2 recovery in MR design as influenced by retentate pressure and operating temperature at steady state. S/C = 3, Q_{liq} = 0.05 ml min^{-1}.

molar flowrates ($F^*_{H_2}$) of produced hydrogen (retentate + permeate) in SR or MR adimensionalized with those obtained without membrane separation (CR) are shown for different pressure values. As expected, the SR configuration showed no influence of the membrane in the production of H_2. In contrast, due to the shift effect originated by the removal of H_2 through the membrane, the MR configuration proved to be clearly superior, with increases of up to 68% in the H_2 production rate. Higher pressure values accentuate the behavior as more hydrogen is permeated through the membrane.

The influence of pressure and temperature on hydrogen recovery, defined as the amount of hydrogen permeated through the membrane divided by the total amount of hydrogen produced, is reported in Fig. 6 for the MR configuration. Hydrogen recovery was strongly dependent on the reactor pressure. The increase of hydrogen recovery through the membrane can be explained in terms of the hydrogen permeation driving force due to the difference in hydrogen pressure at both sides of the membrane, as expected from the Sieverts' law. The larger the pressure difference of hydrogen in the retentate and permeate sides, the larger the hydrogen recovered in the permeate side. However, the increase of pressure produced two conflicting effects. As explained above, a higher hydrogen permeating flux was obtained at higher pressure values but, at the same time, a decrease in the total production of hydrogen due to the thermodynamics of the reaction was observed. Therefore, a plot of the amount of hydrogen recovered against reactor pressure approaches a plateau, as shown in Fig. 6. At pressure values below 12–14 bar, the amount of hydrogen recovered increased with pressure, which means that the membrane effect overcomes the thermodynamic one, while for higher pressure values both effects compensate and the hydrogen recovery is maintained approximately constant. As permeation is a temperature activated process, recovery is also enhanced at increasing temperature, which also favors the thermodynamics of hydrogen formation and, hence, a higher hydrogen partial pressure. High hydrogen recovery values of about 80% were achieved at 873 K.

Fig. 7A shows a comparison of H_2 yield (defined as $F^*_{H_2}/6F_{ETOH}$ according to Eq. (1)) and hydrogen recovery at 773 and 873 K for the MR and SR designs and maintaining a fixed value of the load per unit catalyst mass of Q_{liq}/W_{cat} = 2.3 ml g^{-1} h^{-1} (constant contact time). For both design configurations, an increase of the hydrogen yield with temperature is observed as a result of the thermodynamics of the reforming reaction. For the MR design, the increase in H_2 yield when temperature is increased from 773 to 873 K is higher than that observed for the SR configuration. This is due to the enhancement of the shift effect in the MR design as hydrogen is permeated through the membrane in the reaction zone. It should be noted that at 873 K a remarkable value of 5.1 for the hydrogen yield was obtained, which means ca. 85% with respect to the maximum stoichiometrically possible of 6 (see Eq. (1)). Regarding hydrogen recovery, an enhancement of this variable with temperature is observed for both designs due to both the activation of the membrane and the higher amount of hydrogen produced by the reaction. As expected, hydrogen recovery in the MR design is higher than that corresponding to the SR configuration due to both the superior H_2 yield and the shift effect in the MR configuration.

Fig. 7B presents a similar comparison of the performance of both designs (i.e., H_2 yield and recovery vs. T) based on a constant feed load per unit membrane area of Q_{liq}/A_{memb} = 0.42 ml cm^{-2} h^{-1}. Similar effects than those already discussed above are obtained, that is, an enhancement of hydrogen yield and recovery at increasing temperature due to membrane and reaction kinetic activation. Besides, the effect of the improvement in total hydrogen generation due to the shift as hydrogen is permeated from the reaction medium in the CM configuration is also observed. However, the quantitative differences between performances of MR and SR designs are more moderated on this comparison basis because the MR configuration was loaded with a lower catalyst mass to maintain a constant Q_{liq}/A_{memb} value. Nevertheless, this adverse effect is overcompensated by the hydrogen

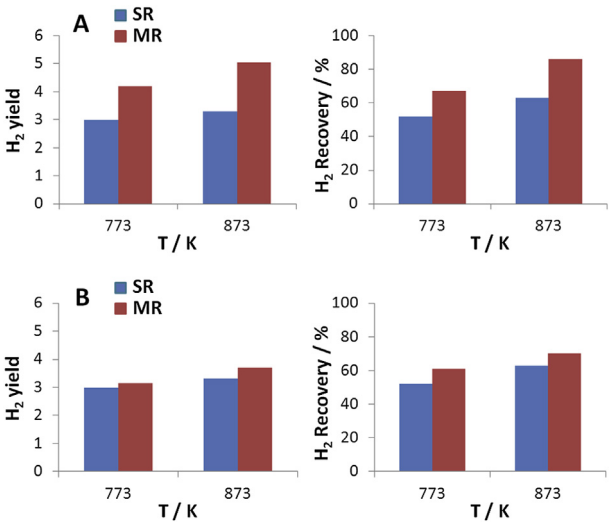

Fig. 7 – Comparison of H_2 yield and recovery under steady state at 12 bar, S/C = 3 and two different temperatures for both MR and SR designs: (A) Q_{liq}/W_{cat} = 2.3 ml g^{-1} h^{-1}; (B) Q_{liq}/A_{memb} = 0.42 ml cm^{-2} h^{-1}.

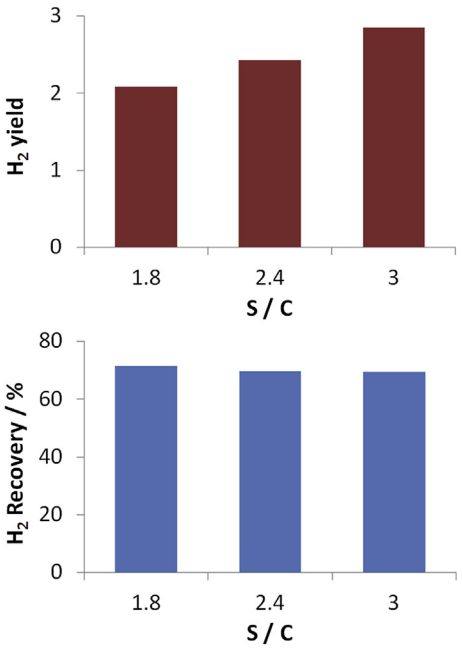

Fig. 8 – Influence of S/C on H_2 yield and recovery at steady state. MR configuration, P = 14 bar, T = 823 K, Q_{liq}/W_{cat} = 6.5 ml g^{-1} h^{-1}.

permeation effect. In these terms, the MR design is capable to attain superior performance parameters than the SR even operating with ca. 1/3 of the catalyst load.

Finally, the effect of the S/C was tested at 823 K for the MR configuration at a constant space velocity of 6.5 ml_{liq} g^{-1} h^{-1} (Fig. 8). As the S/C ratio increases, the hydrogen yield also increases as higher amounts of water shift the equilibrium to render extra hydrogen, as expected from Eqs. (3), (4) and (6). However, as the steam-to-carbon ratio increases from 1.8 up to 3, the amount of unreacted steam in the MR also increases because the stoichiometric S/C ratio for ESR is 1.5 (Eq. (1)). This excess of steam, although beneficial for the production of hydrogen, has a dilution effect in the MR. Then, as the S/C ratio increases, the partial pressure of hydrogen decreases and, consequently, the driving force for the permeation through the membrane decreases and the recovery of hydrogen is lower.

At the end of the experiments (after 650 h of operation at 673–873 K, 1–14 bar and S/C = 1.8–3), the performances of the catalyst and the CMR were maintained intact. This was checked by randomly repeating experiments under several operation conditions. The selectivity and hydrogen recovery values were virtually identical as those recorded previously for each condition. This stable catalytic operation together with the absence of carbon deposition as deduced from SEM and XPS analysis demonstrate the robustness of operation of cobalt hydrotalcite-derived catalysts doped with potassium in a catalytic membrane reactor for producing PEM fuel cell-grade hydrogen from the steam reforming of ethanol in practical applications.

Conclusions

Cobalt hydrotalcite $[Co_2Mg_4Al_2(OH)_{16}]CO_3 \cdot 4H_2O$-derived catalyst doped with potassium was supported over cordierite pieces and placed inside a membrane reactor with a single, dead-end Pd–Ag membrane selective to hydrogen in two configurations. In one configuration, the catalyst pieces were placed in-series with the membrane, forming a staged membrane reactor. In the second configuration, the same catalyst was packed around the membrane, leading to a catalytic membrane reactor. Ethanol steam reforming was carried out in both design configurations at different temperatures, pressures, feed loads and steam-to-carbon values. No sweep gas was used, therefore, pure hydrogen was obtained in the permeate stream, which was maintained at atmospheric pressure. The catalytic membrane reactor configuration showed higher hydrogen yields and hydrogen recoveries than the staged design as resulting from the equilibrium displacement due to the hydrogen removal from the reaction medium. At the conditions tested, the retentate pressure showed a stronger influence on hydrogen yield and recovery than the operating temperature. At 12 bar, 873 K and S/C = 3, 3.7 STP $L_{H_2,\ permeate}$ $mL_{ETOH,\ liquid}^{-1}$ g_{cat}^{-1} were measured for the catalytic membrane reactor, ca. three times higher than the values observed for the staged membrane reactor. The cobalt hydrotalcite-derived catalyst used in the reactor, in both design configurations, exhibited a very stable operation and no carbon accumulation occurred under operation for 650 h, as deduced from SEM and XPS analysis. For the first time, long-term stable operation of a cobalt-based catalyst for ethanol steam reforming at moderate temperature in a catalytic membrane reactor has been demonstrated.

Acknowledgments

This work has been funded through grants Ministry of Economy and Competitiveness ENE2012-36368, PRI-AIBAR-2011-

1092 and MINCYT-MICINN ES/11/07. R.E. acknowledges CONACYT-México for a PhD grant. J.L. and F.M. are grateful to ICREA Academia program.

REFERENCES

[1] Kolb G. Fuel processing for fuel cells. Weinheim: Wiley-VCH; 2008.

[2] Llorca J. Microreactors for the generation of hydrogen from ethanol. In: Lee WH, Cho VG, editors. Handbook of sustainable energy. Nova Publishers; 2010. pp. 693–9.

[3] Murdoch M, Waterhouse GIN, Nadeem MA, Metson JB, Keane MA, Howe RF, et al. The effect of gold loading and particle size on photocatalytic hydrogen production from ethanol over Au/TiO2 nanoparticles. Nat Chem 2011;3:489–92.

[4] Llorca J. Energy from hydrogen. Hydrogen from renewable fuels for portable applications. Contributions Sci 2011;7:57–64.

[5] Vaidya PD, Rodrigues AE. Insight into steam reforming of ethanol to produce hydrogen for fuel cells. Chem Eng J 2006;117:39–44.

[6] Haryanto A, Fernando S, Murali N, Adhikari S. Current status of hydrogen production techniques by steam reforming of ethanol: a review. Energy & Fuels 2005;19:2098–106.

[7] Ni M, Leung YC, Leung MKH. A review on reforming bio-ethanol for hydrogen production. Int J Hydrogen Energy 2007;32:3238–47.

[8] Llorca J, Cortés V, Divins NJ, Olivera R, Taboada E. Hydrogen from bioethanol. In: Gandía LM, Arzamendi G, Diéguez PM, editors. Renewable hydrogen technologies. Amsterdam: Elsevier; 2013. pp. 135–69.

[9] Deluga GA, Salge JR, Schmidt LD, Verykios XE. Renewable hydrogen from ethanol by autothermal reforming. Science 2004;303:993–7.

[10] Frusteri F, Freni S. Bio-ethanol, a suitable fuel to produce hydrogen for a molten carbonate fuel cell. J Power Sources 2007;173:200–9.

[11] Idriss H, Scott M, Llorca J, Chan SC, Chiu W, Sheng PY, et al. A phenomelogical study of the metal-oxide interface: the role of catalysis in hydrogen production from renewable resources. ChemSusChem 2008;1:905–10.

[12] Mattos LV, Jacobs G, Davis BH, Noronha FB. Production of hydrogen from ethanol: review of reaction mechanism and catalyst deactivation. Chem Rev 2012;112:4094–123.

[13] Llorca J, Homs N, Sales J, Ramírez de la Piscina P. Efficient production of hydrogen over supported cobalt catalysts from ethanol steam reforming. J Catal 2002;209:306–17.

[14] Llorca J, Ramírez de la Piscina P, Dalmon JA, Sales J, Homs N. CO-free hydrogen from steam-reforming of bioethanol over ZnO-supported cobalt catalysts. Effect of the metallic precursor. Appl Catal B Environ 2003;43:355–69.

[15] Freni S, Cavallaro S, Mondello N, Spadaro L, Frustreri F. Production of hydrogen for MC fuel cell by steam reforming of ethanol over MgO supported Ni and Co catalysts. Catal Commun 2003;4:259–68.

[16] Mariño F, Baronetti G, Jobbagy M, Laborde M. Cu-Ni-K/γ-Al2O3 supported catalysts for ethanol steam reforming: formation of hydrotalcite-type compounds as a result of metal-support interaction. Appl Catal A General 2003;238:41–54.

[17] Llorca J, Homs N, Sales J, Fierro JLG, Ramírez de la Piscina P. Effect of sodium addition on the performance of Co-ZnO-based catalysts for hydrogen production from bioethanol. J Catal 2004;222:470–80.

[18] Llorca J, Homs N, Ramírez de la Piscina P. *In-situ* DRIFT-Mass spectrometry study of the ethanol steam-reforming reaction over carbonyl-derived Co/ZnO catalysts. J Catal 2004;227:556–60.

[19] Batista MS, Santos RKS, Assaf EM, Assaf JM, Ticianelli EA. High efficiency steam reforming of ethanol by cobalt-based catalysts. J Power Sources 2004;134:27–32.

[20] Kaddouri A, Mazzocchia C. A study of the influence of the synthesis conditions upon the catalytic properties of Co/SiO_2 or Co/Al_2O_3 catalysts used for ethanol steam reforming. Catal Commun 2004;5:339–45.

[21] Song H, Zhang L, Watson RB, Braden D, Ozkan U. Investigation of bio-ethanol steam reforming over cobalt-based catalysts. Catal Today 2007;129:346–54.

[22] Benito M, Padilla R, Rodríguez L, Sanz JL, Daza L. Zirconia supported catalysts for bioethanol steam reforming: effect of active phase and zirconia structure. J Power Sources 2007;169:167–76.

[23] Tutti S, Pepe F. On the catalytic activity of cobalt oxide for steam reforming of ethanol. Catal Lett 2008;122:196–203.

[24] Song H, Ozkan U. Ethanol steam reforming over Co-based catalysts: role of oxygen mobility. J Catal 2009;261:66–74.

[25] Casanovas A, de Leitenburg C, Trovarelli A, Llorca J. Catalytic monoliths for ethanol steam reforming. Catal Today 2008;138:187–92.

[26] Casanovas A, Saint-Gerons M, Griffon F, Llorca J. Autothermal generation of hydrogen from ethanol in a microreactor. Int J Hydrogen Energy 2008;33:1827–33.

[27] Llorca J, Casanovas A, Trifonov T, Rodríguez A, Alcubilla R. First use of macroporous silicon loaded with catalyst film for a chemical reaction: a microreformer for producing hydrogen from ethanol steam reforming. J Catal 2008;255:228–33.

[28] Wang H, Ye JL, Liu Y, Li YD, Qin YN. Steam reforming of ethanol over Co_3O_4/CeO_2 catalysts prepared by different methods. Catal Today 2007;129:305–12.

[29] Sun J, Qiu XP, Wu F, Zhu WT. H_2 from steam reforming of ethanol at low temperature over Ni/Y_2O_3, Ni/La_2O_3 and Ni/Al_2O_3 catalysts for fuel-cell applications. Int J Hydrogen Energy 2005;30:437–45.

[30] Galetti AE, Gomez MF, Arrua LA, Marchi AJ, Abello MC. Study of CuCoZnAl oxide as catalyst for the hydrogen production from ethanol reforming. Catal Commun 2008;9:1201–8.

[31] Vargas JC, Libs S, Roger AC, Kiennemann A. Study of Ce-Zr-Co fluorite-type oxide as catalysts for hydrogen production by steam reforming of bioethanol. Catal Today 2005;107:417–25.

[32] Casanovas A, Domínguez M, Ledesma C, López E, Llorca J. Catalytic walls and micro-devices for generating hydrogen by low temperature steam reforming of ethanol. Catal Today 2009;143:32–7.

[33] López E, Irigoyen A, Trifonov T, Rodríguez A, Llorca J. A million-channel reformer on a fingertip: moving down the scale in hydrogen production. Int J Hydrogen Energy 2010;35:3472–9.

[34] Casanovas A, Roig M, de Leitenburg C, Trovarelli A, Llorca J. Ethanol steam reforming and water gas shift over Co/ZnO catalytic honeycombs doped with Fe, Ni, Cu, Cr and Na. Int J Hydrogen Energy 2010;35:7690–8.

[35] Bichon P, Haugom G, Venvik HJ, Colmen A, Blekkan EA. Steam reforming of ethanol over supported Co and Ni catalysts. Top Catal 2008;49:38–45.

[36] Domínguez M, Taboada E, Molins E, Llorca J. Co-SiO_2 aerogel-coated catalytic walls for the generation of hydrogen. Catal Today 2008;138:193–7.

[37] Domínguez M, Cristiano G, López E, Llorca J. Ethanol steam reforming over cobalt talc in a plate microreactor. Chem Eng J 2011;138:176–7.

[38] Domínguez M, Taboada E, Idriss H, Molins E, Llorca J. Fast and efficient hydrogen generation catalyzed by cobalt talc nanolayers dispersed in silica aerogel. J Mater Chem 2010;20:4875–83.
[39] Espinal R, Taboada E, Molins E, Chimentao RJ, Medina F, Llorca J. Cobalt hydrotalcite for the steam reforming of ethanol with scarce carbon production. Royal Soc Chem Adv 2012;2:2946–56.
[40] Espinal R, Taboada E, Molins E, Chimentao RJ, Medina F, Llorca J. Cobalt hydrotalcites as catalysts for bioethanol steam reforming. The promoting effect of potassium on catalyst activity and long-term stability. Appl Catal B Environ 2012;127:59–67.
[41] Gallucci F, Basile A. Pd–Ag membrane reactor for steam reforming reactions: a comparison between different fuels. Int J Hydrogen Energy 2008;33:1671–87.
[42] Basile A. Hydrogen production using Pd-based membrane reactors for fuel cells. Top Catal 2008;51:107–22.
[43] Mendes D, Tosti S, Borgognoni F, Mendes A, Madeira LM. Integrated analysis of a membrane-based process for hydrogen production from ethanol steam reforming. Catal Today 2010;156:107–17.
[44] Tosti S, Bettinali L. Diffusion bonding of Pd–Ag rolled membranes. J Mater Sci 2004;39:3041–6.
[45] Tosti S, Basile A, Bettinali L, Borgognoni F, Chiaravalloti F, Gallucci F. Long-term tests of Pd–Ag thin wall permeator tube. J Membr Sci 2006;284:393–7.
[46] Tosti S, Basile A, Bettinali L, Borgognoni F, Gallucci F, Rizzello C. Design and process study of Pd membrane reactors. Int J Hydrogen Energy 2008;33:5098–105.
[47] Burkhanov GS, Gorina NB, Kolchugina NB, Roshan NR. Palladium-based Alloy membranes for separation of high purity hydrogen from hydrogen-containing gas mixtures. Platin Met Rev 2011;55:3–12.
[48] Montané D, Bolshak E, Abelló S. Thermodynamic analysis of fuel processors based on catalytic-wall reactors and membrane systems for ethanol steam reforming. Chem Eng J 2011;175:519–33.
[49] Gallucci F, Basile A, Tosti S, Iulianelli A, Drioli E. Methanol and ethanol steam reforming in membrane reactors: an experimental study. Int J Hydrogen Energy 2007;32:1201–10.
[50] Tosti S, Basile A, Borgognoni F, Capaldo V, Cordiner S, Di Cave S, et al. Low temperature ethanol steam reforming in a Pd-Ag membrane reactor: part 1: Ru-based catalyst. J Membr Sci 2008;308:250–7.
[51] Tosti S, Basile A, Borgognoni F, Capaldo V, Cordiner S, Di Cave S, et al. Low-temperature ethanol steam reforming in a Pd–Ag membrane reactor: Part 2. Pt-based and Ni-based catalysts and general comparison. J Membr Sci 2008;308:258–63.
[52] Yu CY, Lee DW, Park SJ, Lee KY, Lee KH. Ethanol steam reforming in a membrane reactor with Pt-impregnated Knudsen membranes. Appl Catal B Environ 2009;86:121–6.
[53] Tosti S, Fabbricino M, Moriani A, Agatiello G, Scudieri C, Borgognoni F, et al. Pressure effect in ethanol steam reforming via dense Pd-based membranes. J Membr Sci 2011;377:65–74.
[54] Papadias DD, Lee SHD, Ferrandon M, Ahmed S. An analytical and experimental investigation of high-pressure catalytic steam reforming of ethanol in a hydrogen selective membrane reactor. Int J Hydrogen Energy 2010;35:2004–17.
[55] López E, Divins NJ, Llorca J. Hydrogen production from ethanol over Pd–Rh/CeO_2 with a metallic membrane reactor. Catal Today 2012;193:145–50.
[56] Iulianelli A, Basile A. An experimental study on bio-ethanol steam reforming in a catalytic membrane reactor. Part I: temperature and sweep-gas flow configuration effects. Int J Hydrogen Energy 2010;35:3170–7.
[57] Iulianelli A, Liguori S, Longo T, Tosti S, Pinacci P, Basile A. An experimental study on bio-ethanol steam reforming in a catalytic membrane reactor. Part II: reaction pressure, sweep factor and WHSV effects. Int J Hydrogen Energy 2010;35:3159–64.
[58] Lim H, Gu Y, Oyama ST. Reaction of primary and secondary products in a membrane reactor: studies of ethanol steam reforming with a silica-alumina composite membrane. J Membr Sci 2010;351:149–59.
[59] Lim H, Gu Y, Oyama ST. Studies of the effect of pressure and hydrogen permeance on the ethanol steam reforming reaction with palladium- and silica-based membranes. J Membr Sci 2012;396:119–27.
[60] Yun S, Lim H, Oyama ST. Experimental and kinetic studies of the ethanol steam reforming reaction equipped with ultrathin Pd and Pd-Cu membranes for improved conversion and hydrogen yield. J Membr Sci 2012;409-410:222–31.
[61] Basile A, Pinacci P, Iulianelli A, Broglia M, Drago F, Liguori S, et al. Ethanol steam reforming reaction in a porous stainless steel supported palladium membrane reactor. Int J Hydrogen Energy 2011;36:2029–37.
[62] Seelam PK, Liguori S, Iulianelli A, Pinacci P, Calabrò V, Huuhtanen M, et al. Hydrogen production from bio-ethanol steam reforming reaction in a Pd/PSS membrane reactor. Catal Today 2012;193:42–8.
[63] Domínguez M, Taboada E, Molins E, Llorca J. Ethanol steam reforming at very low temperature over cobalt talc in a membrane reactor. Catal Today 2012;193:101–6.
[64] Gao H, Lin YS, Li Y, Zhang B. Chemical stability and its improvement of palladium-based metallic membranes. Ind Eng Chem Res 2004;43:6920–30.
[65] Sanz R, Calles JA, Alique D, Furones L, Ordóñez S, Marín P, et al. Preparation, testing and modeling of hydrogen selective Pd/YSZ/SS composite membrane. Int J Hydrogen Energy 2011;36:15783–93.
[66] Gao H, Lin JYS, Li Y, Zhang B. Electroless plating synthesis, characterization and permeation properties of Pd–Cu membranes supported on ZrO_2 modified porous stainless steel. J Membr Sci 2005;265:142–52.
[67] Pinacci P, Broglia M, Valli C, Capannelli G, Comite A. Evaluation of the water gas shift reaction in a palladium membrane reactor. Catal Today 2010;156:165–72.